Journal of Power Sources 218 (2012) 221–232

Contents lists available at SciVerse ScienceDirect

Journal of Power Sources

journal homepage: www.elsevier.com/locate/jpowsour

Experimental characterization of the water transport properties of PEM fuel cells diffusion media

Bladimir Ramos-Alvarado [a], Joshua D. Sole [b], Abel Hernandez-Guerrero [a], Michael W. Ellis [b,*]

[a] Department of Mechanical Engineering, University of Guanajuato, Mexico
[b] Department of Mechanical Engineering, Virginia Polytechnic Institute and State University, United States of America

HIGHLIGHTS

- This work presents guidelines to characterize the water transport characteristics of GDL materials for PEM fuel cells.
- An experimental apparatus is designed and used to measure capillary pressure–saturation relationships in GDL materials.
- An experimental apparatus is designed and used to measure relative permeability of GDL materials as a function of liquid water saturation.
- The water transport characteristics of carbon paper Toray 090 are obtained (porosity, capillary pressure curves, absolute permeability, and relative permeability).

ARTICLE INFO

Article history:
Received 6 April 2012
Received in revised form
22 May 2012
Accepted 23 May 2012
Available online 30 May 2012

Keywords:
GDL
PEM fuel cells
Capillary pressure
Permeability
Experimental
Gas diffusion layer

ABSTRACT

A full experimental characterization of the liquid water transport properties of Toray TGP-090 paper is carried out in this work. Porosity, capillary pressure curves (capillary pressure–saturation relationships), absolute permeability, and relative permeability are obtained via experimental procedures. Porosity was determined using two methods, both aimed to obtain the solid volume of the network of fibers comprising the carbon paper. Capillary pressure curves were obtained using a gas displacement porosimeter where liquid water is injected using a syringe pump and the capillary pressure is recorded using a differential pressure transducer. Absolute and relative permeability were also measured with an apparatus designed at Virginia Tech. Absolute permeability was calculated at different flow rates using nitrogen. On the other hand, relative permeability was a more complicated task to carry out giving the complexity (two-phase flow condition) of this property. All of the water transport properties of Toray TGP-090 were studied under the effects of wet-proofing (PTFE treatment) and compression. Some observations were that wet-proofing reduces the porosity of the raw material, increases the hydrophobicity (P_c–S curves), and reduces the permeability of the material. Similar effects were observed for compression, where compressed material exhibited trends similar to those of wet-proofing effects. The results presented here will allow a more accurate modeling of PEMFCs, providing an experimentally verified alternative to the assumptions frequently employed.

1. Introduction

Proton exchange membrane fuel cells (PEMFC) are considered as promising alternative energy conversion devices for future automobiles and stationary applications owing to their high-energy efficiency, competitive power density, low-temperature operation, fast startup and pollution-free characteristics. However, the performance of the PEMFCs needs to be further improved to increase their cost-effectiveness so that they can compete against current power alternatives [1]. Amongst some of the problems that affect the PEM fuel cells performance, the water management issue is one of the most important to be considered. In order to study this problem, considerable research has been undertaken via numerical and experimental work.

Liquid water removal through the porous gas diffusion layers (GDL) of PEM fuel cells has received much attention from the transport phenomena modeling point of view. There are three main approaches for the simulation of water transport through the GDL: direct approach, pore network approach, and continuum medium approach. Of the three approaches, the continuum medium approach is the only one that allows an easy coupling of the water transport model with the species, momentum, energy, and charge transport equations, creating a model that can predict cell

* Corresponding author. Tel.: +1 540 231 9102.
E-mail address: mwellis@vt.edu (M.W. Ellis).

0378-7753/$ – see front matter © 2012 Elsevier B.V. All rights reserved.
doi:10.1016/j.jpowsour.2012.05.069

performance and liquid water saturation distribution in the GDL. Two main modeling schemes can be distinguished in the continuum models. The first one was proposed by Wang and Cheng [2]. These authors present a novel formulation of transport processes based on a multicomponent system for porous media where the liquid and gas phase equations are linked through mixture parameters in order to form single transport equations, this modeling scheme is known as the M^2 model. The second modeling scheme is known as the unsaturated flow theory (UFT); it is based on the assumption that the pressure gradient of the gas phase is negligible in the GDL in comparison with the liquid pressure gradient. The earlier applications of the UFT scheme can be tracked to He et al. [3] and Natarajan and Nguyen [4]. However, regardless of the continuum modeling scheme, both depend upon GDL properties such as porosity, capillary pressure curves (capillary pressure–saturation relationships), and permeability.

Two-phase modeling of PEM fuel cells has been described using continuum media schemes since 2000 [3]; however, it was not until 2006, when Gostick et al. [5] conducted one of the first experimental characterizations of GDL material, obtaining the capillary pressure curves of three of the common types of carbon paper and carbon cloth material used in PEM fuel cells as GDLs. The method of standard porosimetry (MSP) was used to determine the capillary pressure–saturation relationships (P_c–S). The method of standard porosimetry is based on the principle of capillary equilibrium. When two partially saturated porous bodies are in contact, the system moves towards equilibrium where the capillary pressures of the liquid in both bodies are equal. A body with known P_c–S relation is placed in capillary contact with the body of unknown P_c–S relation. Gostick et al. [5] calculated the porosity of the GDL material using mercury intrusion porosimetry (MIP); the capillary pressure curves were obtained using an adaptation of Washburn's equation. This equation is derived for capillary tubes. Finally, using the Von Genuchten and Brooks-Corey approximations, the authors were able to obtain analytical expressions for relative permeability.

In 2007 Fairweather et al. [6] designed an experimental apparatus to obtain the capillary pressure curves of Toray 090 and Avcarb materials. The apparatus consisted of a holding device where the GDL material was placed and sealed while water was injected using a syringe pump operated in a stepwise fashion. Saturation was calculated based on the liquid water injected and the capillary pressure was obtained from a differential pressure transducer after reaching steady-state at each step of the injection process. Fairweather et al. studied the effects of wet-proofing and obtained hysteresis curves of the imbibition-drainage processes. Gostick et al. [7] published a short communication where they reported capillary pressure curves during imbibition and drainage of Toray 090 and SGL10BA GDL. Their novelty was the design of an experimental apparatus to obtain imbibition and drainage curves by controlling the gas phase pressure instead of the liquid phase pressure. Gostick et al. argued that by controlling the gas phase pressure and allowing water to imbibe into the GDL sample, the characterization of imbibition/drainage cycles was more properly conducted than using water injection. One year later, Gostick et al. [8] extended the application of their apparatus to study the effects of compression on capillary pressure curves. These authors studied the effects of wet-proofing and proposed an index to quantify how hydrophobic or hydrophilic a porous material is. The same year, Gostick et al. [9] published a short communication where the application of their apparatus was applied to characterize GDL material with microporous layers. Many of the experimental approaches designed to obtain capillary pressure curves during imbibition and drainage have one similar characteristic, namely, the sample is held between a hydrophilic porous membrane and a hydrophobic porous membrane. Water is added to and removed from this sandwich through the hydrophilic side with air moving in and out of the sample through the hydrophobic membrane on the opposite side. This approach was also employed in the work presented by Harkness et al. [10]. In this work they designed a water porosimeter following a design similar to that of Fairweather et al. [6]; however, the so called water porosimeter operates at a constant injection rate controlled by a syringe pump. Harkness et al. [10] obtained capillary pressure curves at different compression and also addressed the effects of wet-proofing.

The research described in the preceding paragraphs reflect a small but growing body of literature focused on the development of experimentally determined capillary pressure curves of GDL material for fuel cells. Even fewer works are focused on the determination of absolute and relative permeability of GDL materials. Absolute permeability is a property of a porous media and is related to the pressure gradient required to force a single-phase flow through a porous structure. On the other hand, relative permeability is related to a two-phase flow flowing through a porous media. Relative permeability is not a property of a porous media but a function of fluid properties, flow conditions, porous matrix properties, history of the system, etc. Gostick et al. [11] determined the absolute permeability of common GDL carbon paper and carbon cloth in three different directions, addressing the effects of PTFE treatment and compression. More recently, Hussaini and Wang [12] measured absolute permeability and determined liquid and air relative permeability as a function of liquid water saturation of the GDL material, in plane and through plane. The measurement of absolute permeability was found to be a straightforward procedure, unlike the measurement of relative permeability where the authors concluded that only the measurements in plane were reliable and further investigation was required for determining the functions of relative permeability through plane.

More recently, Jörg Roth [13] presented a comprehensive study of the water transport properties of Toray 060 carbon paper with and without wet-proofing. The author developed a novel technique to determine the functional relationship $P_c(S)$. The novel measurement principle is based on the saturation dependent change of the buoyancy of a partially saturated sample immersed into water. The capillary pressure curves obtained by Roth were not comparable to those available in the technical literature; he attributed such differences to the effects of immobile liquid water saturation in the GDL samples. Roth also measures permeability and relative permeability of Toray 060 samples using a pressure-controlled experimental setup instead of the common flow-controlled based experiments [11,12,14]. The same difficulties found by Hussaini and Wang [12] in their measurements of relative permeability were encountered by Roth [13].

In this work the experimental apparatus and procedures designed by Sole [14] are used to determine capillary pressure curves, absolute permeability, and relative permeability of carbon paper Toray 090. The effects of three different PTFE treatments are studied (0%, 10%, and 20%) as well as different compressions. Porosity determination and wet-proofing are conducted on the GDL materials. The sample preparation process for the capillary pressure determination experiment was modified to simplify the procedure originally reported by Sole [14]. The final objective of this work is to provide guidelines for a complete characterization of a GDL material in order to obtain the necessary properties for two-phase flow models of PEM fuel cells.

2. Experimental procedures

In this section, the experimental apparatus and procedures will be described. The main components and operating principles of the experimental apparatus will be discussed in separate subsections.

Likewise, a brief description of the procedures will be outlined in each subsection.

2.1. Wet-proofing and porosimetry

The hydrophobic treatment of gas diffusion media with PTFE has been widely reported in the literature as an enhancing agent of water removal. In this work, Toray 090 carbon paper was studied as delivered by the manufacturer and treated with PTFE using the following procedure: (1) a representative amount of GDL is cut from the sheet stock, weighed, and then treated with an aqueous solution of PTFE; (2) the material is dried in air at 80 °C to evaporate the water to be weighed again, then the mass percent of PTFE is calculated; (3) if the percent of PTFE is appropriate, the treated GDL is heated at 350 °C for 30 minutes to sinter the PTFE on the porous matrix. Following the foregoing steps, treatments of 10% and 20% PTFE were obtained.

Porosity calculation is fundamental in this study in order to have an accurate calculation of the capillary pressure curves and relative permeability relationships. The porosity of untreated and treated material was determined using two methodologies i.e., the gravimetric and the buoyancy method. The gravimetric method basically consists of determining the volume of the solid matrix in the porous media using geometric characteristics and mass of a sample. The steps followed to conduct this procedure are:

1. A sample is cut using a circular die and weighed several times to obtain an average mass of the sample (m_{solid}).
2. The thickness of the sample is measured using a flat-faced thickness gage. Also, the actual diameter of the sample is determined by measuring the diameter of the die using an analytical caliper.
3. The volume of the solid matrix is determined using the following

$$V_{solid} = \frac{m_{solid}}{(1 - \%PTFE)\rho_{carbon} + (\%PTFE)\rho_{PTFE}} \quad (1)$$

4. The uncompressed porosity is determined

$$\varepsilon_o = 1 - \frac{V_{solid}}{A_{sample} t_{sample}} \quad (2)$$

where A_{sample} and t_{sample} are the area and thickness of the sample, respectively.

The buoyancy method consists of applying Archimedes' principle to determine the volume of the solid matrix. A fully wetting fluid is used in order to wet the whole matrix, however, some pores might be trapped and therefore they will be inaccessible to the wetting fluid. The steps followed to conduct this method are:

1. A sample is cut using a circular die.
2. The thickness of the sample is measured using a flat-faced thickness gage. Also, the actual diameter of the sample is determined by measuring the diameter of the die using an analytical caliper.
3. The sample is hanged from the underside hook of a balance until a steady mass reading (m_{dry}), is achieved.
4. The sample is submerged into n-pentane and the mass is measured (m_{wet}). The volume of the solid matrix is determined using the following equation:

$$V_{solid} = \frac{m_{dry} - m_{wet}}{\rho_{n-pen}} \quad (3)$$

5. The uncompressed porosity is determined using Eq. (2).

The Archimedes' principle is observed in Eq. (3), where the volume of the solid matrix is determined based on the weight of the displaced fluid which is equal to the buoyancy force measured by the balance. To obtain an approximation of porosity under compression (ε), Eq. (4) is applied,

$$\varepsilon = \varepsilon_o \frac{t}{t_o} \quad (4)$$

where t_o is the original thickness and t is the compressed thickness.

2.2. Capillary pressure curves

The capillary pressure curves of fuel cells diffusion media was determined using the experimental apparatus designed by Sole [14] but with a modified procedure. The sample preparation procedure employed by Sole uses a hot press step at 320 °C in order to melt a hydrophobic PTFE membrane over the edges of an aluminum sample holder forming a perimeter seal. Sole's sample preparation process precludes the creation of a 3-layer capillary system (hydrophobic–GDL–hydrophilic) due to the high press temperatures, which exceed the fusion temperature of the hydrophilic materials.

In the present work, a sample holder similar to the one reported in Ref. [14] was designed aiming to eliminate the hot press procedure; hence, a hydrophilic membrane can be added to the system presented by Sole. Fig. 1 depicts a 3D view of the modified sample holder. This sample holder is made from aluminum and has an external diameter of 47.6 mm, a thickness of 3.8 mm, flow inlets of 1.6 mm, and can hold samples of 33.3 mm in diameter. The hot press procedure was eliminated by modifying the sealing of the system with an o-ring, as depicted in Fig. 1. The compression effects were studied by modifying the depth of the supporting surface (i.e., the surface with the inlet holes).

The sealing of the system is fundamental in order to obtain accurate results. Fig. 2 shows the sealing detail and the sample preparation. The preparation process of the sample is simple and is accomplished following these steps: (1) a portion of diffusion media (Toray 090) and a piece of hydrophilic material (MAGNA Nylon supported, 1.2 μm, 47 mm) are cut using a standard die of nominal size 33.3 mm; (2) the gas diffusion media and the hydrophilic material are placed on the sample holder as shown in Fig. 2; (3) a hydrophobic membrane (Zefluor supported PTFE, 0.5 μm, 47 mm) is placed on top of the gas diffusion media; (4) an o-ring is placed in the groove by exerting pressure in order to deform the hydrophobic membrane and attaining the wrapping shown in

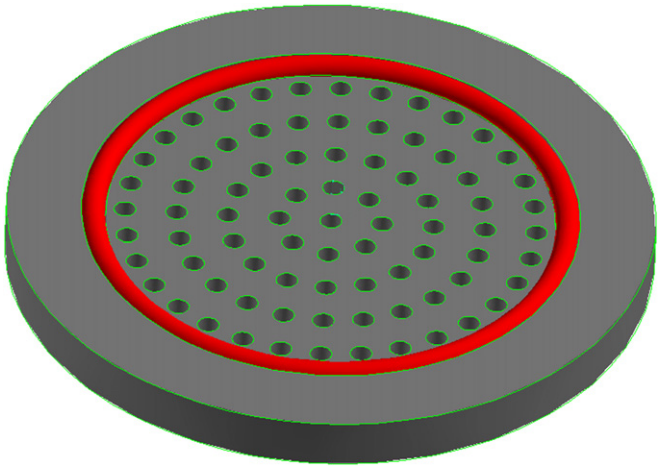

Fig. 1. 3D view of the novel sample holder designed for Sole's apparatus [13].

Fig. 2; (5) the assembly is slightly pressed using a manual hydraulic press to obtain a better seal.

Once the sample has been prepared, the assembly shown in Fig. 2 is placed into the experimental apparatus, as shown in Fig. 3. The procedure followed to obtain a capillary pressure curve is as follows:

1. The sample is placed into the fixture shown in Fig. 3 and a sintered stainless steel retaining ring is placed on top and the ring is well tightened to avoid water leaks around the base of the sample holder.
2. The valves V1 and V2 are open to the atmospheric air and the syringe pump (KD Scientificr Model 200) is started to inject 1 ml of water at 100 $\mu l\,min^{-1}$ to nearly fill the empty volume below the sample holder.
3. Afterwards, the syringe pump is started at 10 $\mu l\,min^{-1}$ and the pressure difference (atmosphere-water) is sensed by pressure transducer G1 (Omega PX-2300-5DI) and is continuously recorded until the high pressure limit of the transducer is reached. The data is recorded in a LabView application connected to a National Instruments data acquisition system.

2.3. Absolute and relative permeability

A two-phase flow system is generated by mixing air and water at known rates in the pre-mixing section shown in Fig. 4. The pre-mixing section consists of a highly hydrophilic material which reduces the size of liquid droplets ensuring an appropriate mixing with the flowing air. The water flow rate is controlled by a syringe pump and the air flow is controlled by a mass flow controller. A PTFE distributor is added at the inlet in order to generate a uniform flow inlet condition. Prior to the two-phase mixture entering the GDL specimen, it passes through a layered section of similar material. This section is added before and after the specimen with the purpose of reducing end effects. Also, different compression magnitudes can be studied by adding more or less layers of material. The saturation of the specimen under study is determined by gravimetric methods as shown in Fig. 4.

The test specimen for both, absolute and relative permeability experiments, is prepared as follows: (1) two pieces of thermoplastic film are cut into a ring shape and placed on the top and bottom of the GDL specimen; (2) the thermoplastic/GDL/thermoplastic sandwich is pressed under light load at 130 °C to fill the porous regions around the perimeter of the GDL, and leave an unfilled region in the center of the GDL specimen; (3) a thin PTFE monofilament is adhered to the edge of the GDL specimen so it can be suspended from the underside hook of an analytical balance.

The GDL mixing layers are prepared by cutting appropriately sized discs of GDL from the same sheet stock used for the central GDL specimen. The appropriate number of layers are bonded together around the perimeter and placed in the recess of the upstream and downstream pipe. To avoid the GDL mixing layers from falling out of the pipe recess when the apparatus is opened, a small diameter monofilament is placed over the surface and pushed under the o-ring on the face of the pipe.

Following the fabrication of the test specimen, and the insertion of the GDL mixing layers in the experimental apparatus, the relative permeability experiment proceeds in the following manner [14]:

1. The mass (m_{dry}), face area (A), and thickness (t) of the GDL specimen is measured.
2. The GDL test specimen is inserted into the fixture and the two sides of the fixture are forced together to ensure a seal at the o-ring/specimen interface on both sides of the GDL specimen.
3. Saturated air is delivered at a constant rate.
4. The flow rate of liquid water ($\dot{V}_l$) is started at a low rate and the pressure differential is monitored over time until steady-state has been achieved. The pressure differential is recorded.
5. The flow is stopped and the two sides of the fixture are separated. The mass of the partially saturated GDL specimen ($m_{partial}$) is measured and recorded.
6. The liquid water saturation (S) is calculated using Eq. (5).

$$S = \frac{1}{\varepsilon A t}\left(\frac{m_{partial} - m_{dry}}{\rho_{water}}\right) \tag{5}$$

7. The relative permeability of the liquid phase ($k_{r,l}$) phase is calculated via Eq. (6).

$$k_{r,l} = \frac{\mu_l n t}{KA\Delta P}\dot{V}_l \tag{6}$$

where the subscript l indicates liquid, t is the thickness of the GDLs, A is the face area of the GDLs, K is the absolute permeability of the media, and n is the number of gas diffusion media layers in the stack.

8. The fixture is closed, the flow is resumed, and the flow rate of liquid water is increased. The pressure differential is monitored until steady-state is reached.
9. Steps 5–8 are repeated until four different points on the k_r–S curve have been measured.

The experimental apparatus shown in Fig. 4 is also suitable to obtain the average value of absolute permeability. In order to do this, the pre-mixing section is removed, no liquid is forced through the specimen, and dry gas is used rather than humid air. Absolute permeability measurement is a straightforward application of Darcy's Law:

$$K = \frac{\mu \dot{V}}{A}\left(\frac{\Delta x}{\Delta P}\right) \tag{7}$$

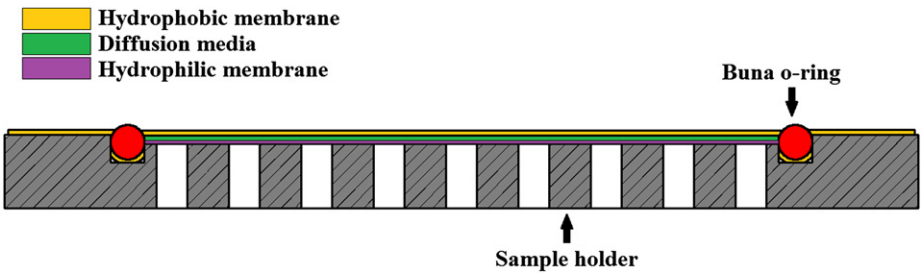

Fig. 2. Sample preparation for the capillary pressure curve experiment.

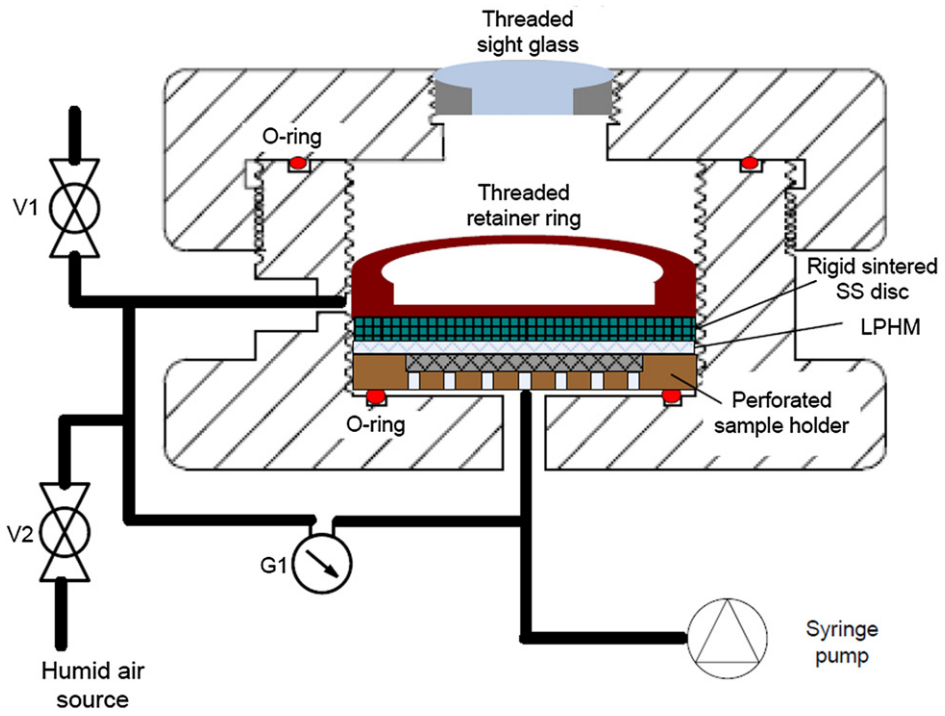

Fig. 3. Experimental apparatus used to determine capillary pressure curves.

where $\dot{V}$ is the volumetric flow rate of dry gas through the gas diffusion layer, μ is the kinematic viscosity of the fluid, A is the flow area, ΔP is the pressure drop caused by the porous structure, and Δx is the thickness of the sample through which the gas flows.

2.4. Effects of immobile liquid water saturation

The liquid water saturation in a porous material is defined as the ratio of the volume occupied by liquid water to the total pore space available. On the other hand, the reduced liquid water saturation is defined in a similar fashion to saturation but taking into account the effects of the immobile liquid water trapped inside dead-ended pores in a porous material (immobile saturation). The immobile saturation can have important effects on the water transport properties like (1) the creation of a more tortuous path to single-phase flow and (2) the modification of the contact angle for a two-phase flow. Such effects have been reported in Ref. [15]. In order to avoid such complications related to the effects of immobile liquid water saturation, a rigorous drying process was conducted on every sample before testing. The samples were repeatedly dried in an oven at conditions of 80 °C for periods of thirty minutes; after each drying, the samples were weighed until a constant mass was

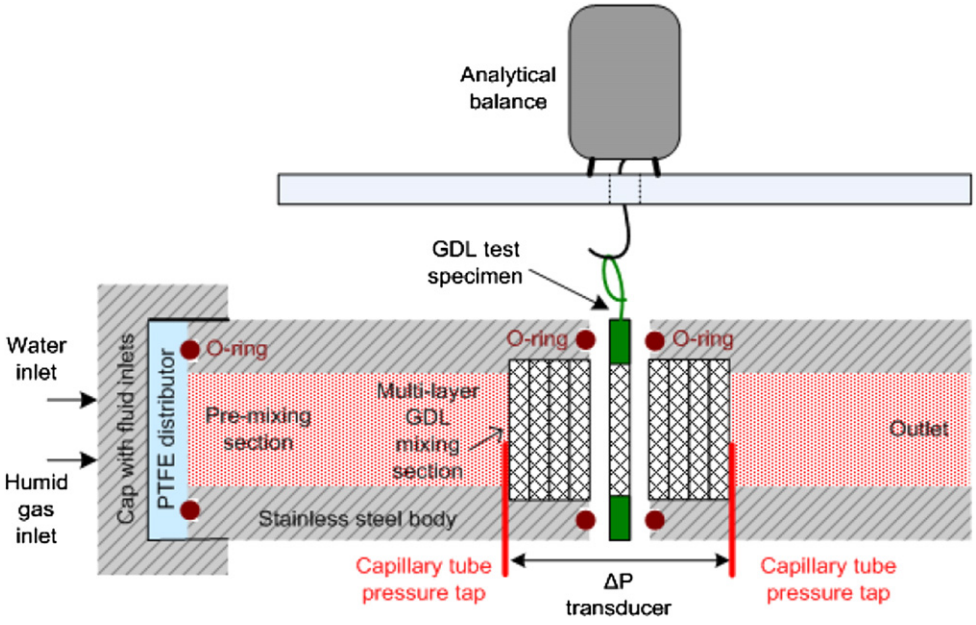

Fig. 4. Diagram of the experimental apparatus to measure permeability designed by Sole [13].

attained. After the constant weight was achieved, the experimental procedures described in the preceding were implemented.

3. Uncertainty analysis

All experimental measurements include non-quantifiable errors during measurement that can be attributed to human interaction as well as, other sources of error that can be expressed by a numerical value. Every parameter determined by a series of measured variables can be expressed as

$$\xi = \xi(\vec{x}) \tag{8}$$

where ξ is the experimentally determined parameter and $\vec{x}$ contains all the measured quantities (sources of uncertainty) involved in the determination of ξ. In this work, the propagation of error approach will be used to determine the uncertainty in the calculation of the diffusion media properties:

$$u(\xi) = \pm\left\{\sum_{i=1}^{n}\left[\frac{\partial\xi}{\partial x_i}u(x_i)\right]^2\right\}^{1/2} \tag{9}$$

where $u(\xi)$ is the uncertainty associated with the determination of the experimental parameter ξ and $u(x_i)$ is the uncertainty of the measurement of the variable x_i.

4. Results

4.1. Porosity

Prior to determining porosity, two large samples of Toray 090 were treated with PTFE in order to make them more hydrophobic. Following the procedures described in Section 2.1, treated materials with 9.16% and 19.74% PTFE content were obtained. From here on, these materials will be referred as 10% and 20% PTFE content. The results of applying the gravimetric and buoyancy methods described in Section 2.1 are shown in Table 1.

Table 1 clearly shows how the PTFE content reduces the average porosity because of the reduction of the pore volume due to the PTFE content in the porous matrix. In other words, the PTFE content occupies some of the available space in the original porous matrix. This trend can be observed in both, gravimetric and buoyancy methods. It is also observed that the gravimetric method predicts larger porosities in all cases. This trend was expected because the buoyancy method does not consider trapped pores inside the matrix; hence, the porosity calculation is lower than that obtained by gravimetric methods. The average porosity was determined by averaging both measurements without including the error propagation. It is observed how the average porosity obtained in these experiments is very similar to the data reported by the manufacturer. Thus, it is concluded that the porosity determination was carried out successfully.

Table 1
Porosity of treated and untreated Toray 090 carbon paper.

Material	Porosity			Manufacturer specifications
	Gravimetric	Buoyancy	Average	
Untreated	0.8 ± 0.0177	0.77 ± 0.015	0.785	0.78
10% PTFE	0.775 ± 0.0181	0.73 ± 0.016	0.752	0.75[a]
20% PTFE	0.757 ± 0.0178	0.705 ± 0.016	0.731	0.73[a]

[a] Reported as manufacturer specifications by Gostick et al. [8].

4.2. Capillary pressure curves

The sample holder design shown in Fig. 2, allows a full sample preparation outside the experimental fixture and avoids the hot press procedure reported in the original design by Sole [14]. The actual compressed thickness of the GDL sample cannot be directly obtained due to the stacking of three different materials (hydrophobic membrane, GDL, and hydrophilic membrane). However, the thickness of the whole assembly is known under the compression of the retainer ring because the edges of the holding section limit the displacement of the sintered metal disk. Also, while the compression force of the retainer ring is not known, it is known that all the materials are subjected to the same force.

A compression compliance study was carried out in order to determine the deformation of the hydrophobic membrane, gas diffusion media, and hydrophilic membrane under compression. The compliance experiment was carried out using a dynamic mechanical analyzer (DMA-Q800 TA Instruments). Circular samples of diameter 12.7 mm were stacked until obtaining a thickness around 2 mm. Then, the samples were placed in the compression clamps of the DMA after carrying out all the pertinent calibrations. The experiments were conducted using the controlling software provided by the manufacturer. Using the software, thickness and diameter of the stacked samples were supplied. A constant strain rate of 5% min^{-1}, a final strain of 50%, and room temperature were selected as the experimental conditions. Fig. 5 shows the results of the compression compliance study, with this information it is possible to determine the compression of the GDL based on the total thickness of the 3-layer assembly and the assumption that all layers experience the same force.

The pressure sensor used to record capillary pressure curves was a differential pressure transducer with a capacitive sensor. The operating principle of this device involves measuring the variation of capacitance of a capacitive system while displacing one of the plates by the action of pressure. The compliance of the pressure transducer was obtained by a simple experimental procedure. The inlet port of the experimental fixture was dead-ended and water was imbibed and drained several times until the compliance relationship indicated in Fig. 6 was established.

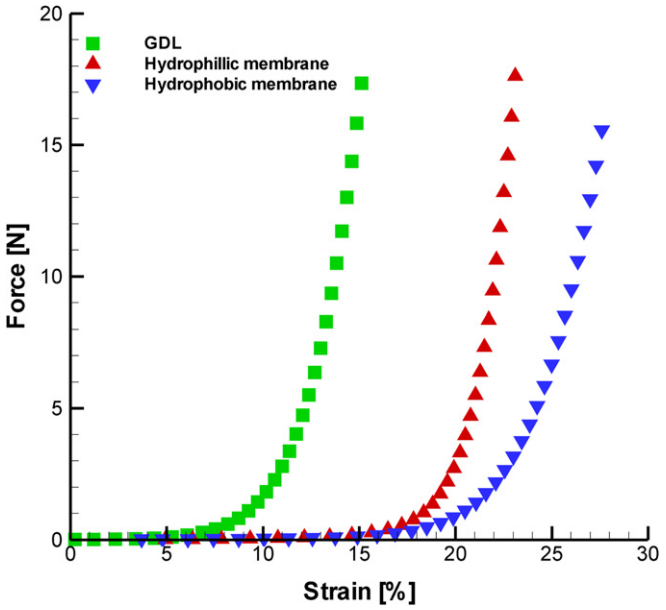

Fig. 5. Compression compliance study.

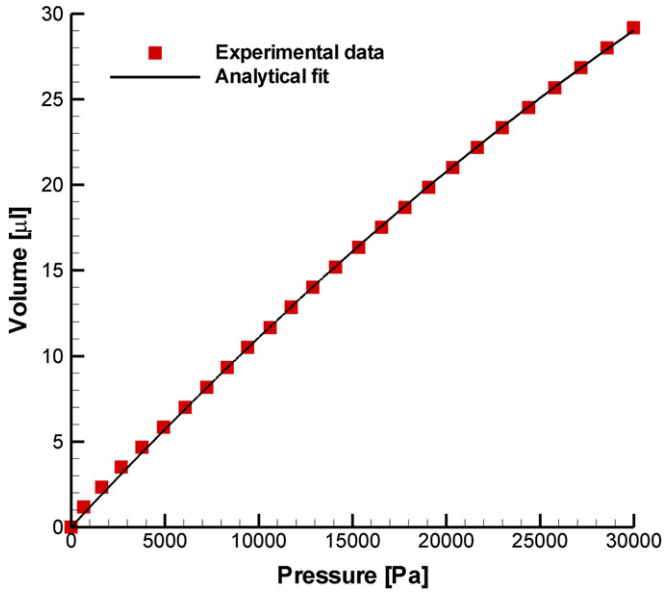

Fig. 6. Pressure transducer compliance.

Fig. 6 presents the experimental results and an analytical expression for the compliance volume that can be subtracted from the total water supplied to determine the actual water intruded into the GDL material. It was found that a 2nd order polynomial function was accurate enough to represent these data.

$$\Delta V_{\text{trans}} = 1.1788 \times 10^{-3} P - 7.0576 \times 10^{-9} P^2 \tag{10}$$

where ΔV_{trans} is the compliance of the diaphragm in μl and P is the pressure recorded by the transducer in Pa. The analytical fitting presented in Eq. (10) was forced to go through the origin in order to have a more realistic representation of the physical phenomenon studied.

The calculation of the saturation of the GDL materials was determined by obtaining the ratio of the water volume imbibed into the material and the available void volume of the compressed media. Eq. (11) shows the expression for calculating saturation:

$$S = \frac{\Delta V_{\text{pump}} - \Delta V_{\text{trans}}}{\frac{\pi}{4} D^2 t \left(\varepsilon_o \frac{t}{t_o} \right)} \tag{11}$$

where ΔV_{pump} is the water volume injected by the syringe pump, ΔV_{trans} is the compliance of the pressure transducer, D, t, t_o, and ε_o are the diameter, actual thickness, uncompressed thickness and uncompressed porosity of the GDL sample, respectively. All of the variables included in the expression for determining saturation have an associated degree of uncertainty either due to manufacturing processes or to operating conditions. Table 2 shows the uncertainty values used in the error propagation analysis.

Table 2
Uncertainty values for saturation determination in the capillary pressure curves experiment.

Uncertainty	Value	Units	Notes
$u(\Delta V_{\text{pump}})$	1.4	μl	Measured
$u(\Delta V_{\text{trans}})$	Pressure dependent	μl	See Fig. 6
$u(D)$	0.01	mm	Manufacturer specs.
$u(t)$	0.0125	mm	Machining tolerance
$u(t_o)$	0.0005	mm	Manufacturer specs.
$u(\varepsilon_o)$	Material dependent	–	See Section 4.1

It can be observed that the uncertainty in the saturation calculation depends upon pressure and the GDL material used. In regards to the syringe pump uncertainty note, it must be clarified that a minute leak was detected in the sample holder assembly. This leak was not eliminated but it was measured and included as an uncertainty in the calculations. Finally, the error associated with the pressure measurement was obtained from the manufacturer specifications of the transducer, this uncertainty is $u(\Delta P) = 86.2$ Pa. The collected uncertainty calculated for saturation was ±8%.

The repeatability of the capillary pressure curves experiments was tested for every material in order to determine the reliability of the data obtained from the experiments. The results reported in the following section are the average value of the different replicates. Fig. 7 shows the repeatability of an experiment using a sample with 20% of PTFE under a compression of 23.2%. The curves presented in Fig. 7 are plotted in terms of raw data without eliminating the transducer compliance. Results shown in Fig. 7 are representative of the repeatability obtained for two different experiments. These results suggest a repeatable and reliable experimental procedure.

Fig. 8 depicts a comparison of capillary pressure curves during imbibition obtained in the present study and the results obtained by Gostick et al. [8]. Both curves were acquired for the same material (Toray 090) in an untreated state as delivered by the manufacturer. A good agreement between both studies is observed in Fig. 8. It must be highlighted that the experimental apparatus used in Ref. [8] is completely different than the one used in this work. The Gostick et al. experimental apparatus controls the gas phase pressure instead of the liquid phase pressure as a manner to manipulate capillary pressure; nonetheless, both curves obtained by different methods are very similar. As it was discussed in Ref. [16], the gas phase controlling method allows a better observation of the asymptotic behavior of the capillary pressure curves at saturation levels near 1. Such a behavior is observed in Fig. 8 when comparing both curves.

Fig. 9 presents the effect of wet-proofing on GDL carbon paper material Toray 090 under a compression of 23.2%. An isobar (6000 Pa) is drawn in Fig. 9 to show the impact of wet-proofing on the capillary pressure curves of the gas diffusion material. It can be observed that an untreated porous material is nearly saturated (87%), whereas a material with a 10% of PTFE only has a saturation

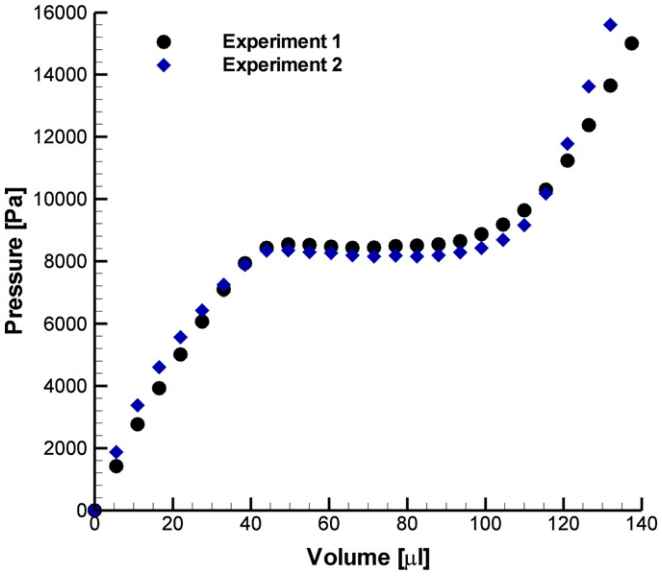

Fig. 7. Repeatability of capillary pressure curves experiment.

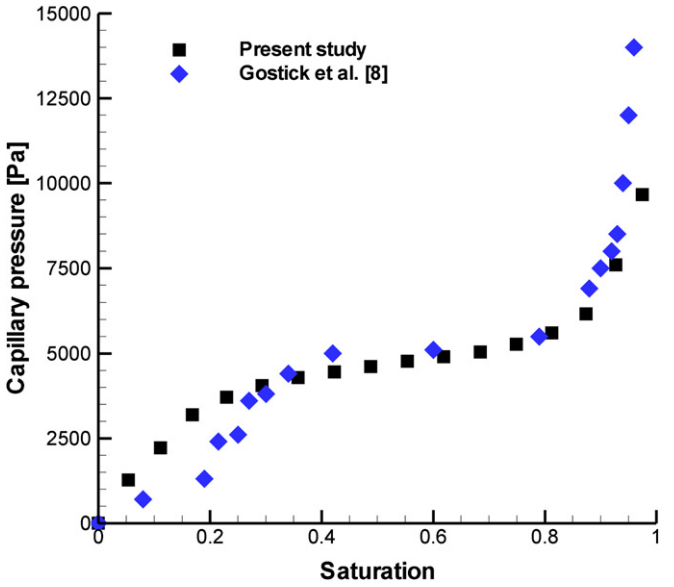

Fig. 8. Comparison of between the capillary pressure curves obtained in this work and a previous study.

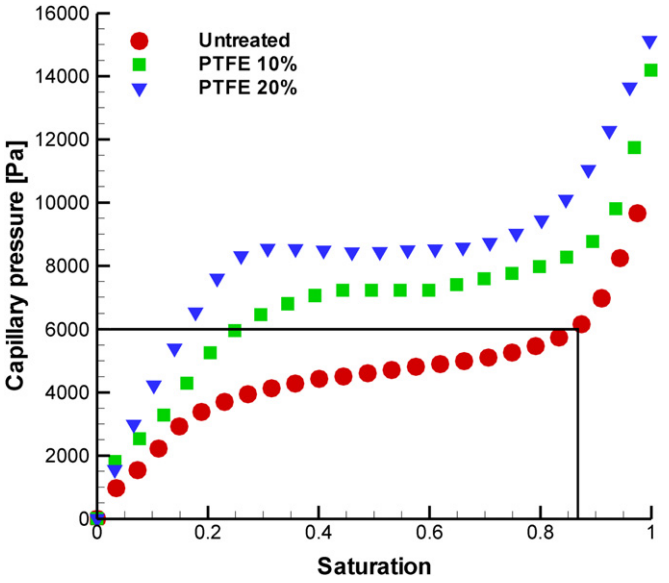

Fig. 9. Effect of PTFE on capillary pressure curves.

of 22%, and a material with 20% of PTFE has an even lower saturation of 17%.

There are three regions that can be readily observed in every capillary pressure curve regardless of the characteristics of the material. The first region of the curves is a sudden increase of capillary pressure until a saturation of nearly 20% is achieved. This region represents the filling of the pores near the surface where the porosity differs from the average size distribution due to the roughness of the surface. The second region of the capillary pressure curves is a plateau where the capillary pressure remains nearly constant while the water saturation increases almost to 80%. This plateau represents the filling of the average pore size of each material. The final region of the capillary pressure curves is a steep increase in capillary pressure owed to the reduction of available pore space for the imbibing water, due to the nearly complete saturation of the porous matrix. This part of the curves should be represented mathematically by an asymptotic behavior; however, the continuous injection of water does not allow observing such a characteristic. The same issue about continuous injection methods was mentioned by Gostick et al. [16].

Fig. 10(a) shows the effect of compression, accomplished using different sample holders, on capillary pressure curves for non-wet-proof material. Three different levels of compression were studied: 5.23% (nominally uncompressed material), 23.2%, and 30.25%. The three compressions are related to the percentage of deformation of a sample of Toray 090. It can be observed in Fig. 10(a) that compression has a significant effect on capillary pressure curves. It is shown that an uncompressed GDL allows more water to imbibe at a given capillary pressure than a compressed material. Such a behavior can be explained due to the effect of reduction of the available pore size and space. A compressed material has less available pore space, lower porosity, and exhibits a more intricate pattern to a given flow.

Fig. 10(b) depicts the effect of compression on wet-proofed material with a PTFE content of 20%. The wet-proofing of the GDL material makes the carbon fibers more hydrophobic and, also reduces the available pore space due to the deposition of PTFE. Hence, compression is expected to show a similar effect on capillary pressure curves for treated material like the one observed for untreated material. Fig. 10(b) shows the effect of the reduction of pore size when the GDL material is compressed from 23.2% to

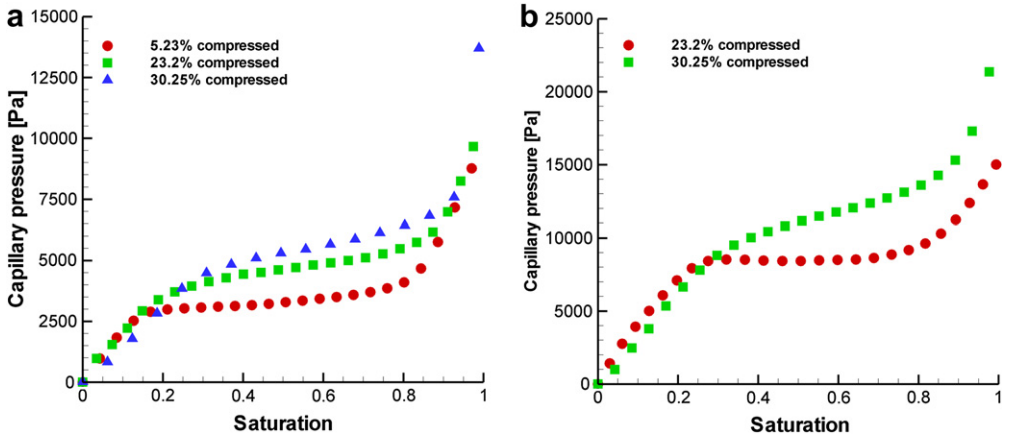

Fig. 10. Effect of compression on capillary pressure curves, (a) non-wet-proof material and (b) wet-proof material (20% of PTFE).

30.25%. The capillary pressure curve with a compression of 30.25% does not show the plateau-like region where the average pore size of the GDL is filled with water. Plateaus are observed in both, Fig. 10(a) and (b). The absence of this plateau can be attributed to the breaking of some fibers due to the compression during experiments.

4.3. Absolute permeability

The calculation of absolute permeability is a straightforward application of Darcy's equation. Under a single-phase condition, absolute permeability can be determined by:

$$K = \frac{\mu \dot{V}}{A}\left(\frac{\Delta x}{\Delta P}\right) \tag{12}$$

this equation can be rearranged in terms of pressure gradients and superficial velocity as:

$$\frac{\Delta P}{\Delta x} = \frac{\mu v_s}{K} \tag{13}$$

where it can be clearly seen that absolute permeability can be obtained as the normal to the curve resulting from the relationship shown in Eq. (13); in other words, absolute permeability can be obtained by calculating the reciprocal of the slope of the curve. Under low Reynolds number conditions this relationship is linear. The sources of uncertainties in the determination of absolute permeability can be deducted from Eq. (12), namely, geometric parameters, pressure, and flow measurements. The uncertainties values used in the analysis of error propagation are summarized in Table 3.

Absolute permeability is a material property related to the ability of a fluid to flow through a porous media. A high value of absolute permeability is associated with a material that presents few obstacles to the flow a single-phase fluid. Hence, effects such as compression have a significant effect on this parameter. Fig. 11 shows the effects of compression on absolute permeability for an untreated sample of Toray 090. As it was stated in Eq. (13), absolute permeability is calculated as the reciprocal of the slope of the data presented in Fig. 11. It is observed how a compressed material has a lower absolute permeability than an uncompressed material. This can be explained due to the reduction of the available pore space, and the resulting generation of a more tortuous path to the flow by compressing a porous media. The calculated permeabilities were $K_{4\%} = 11.96 \pm 0.5 \times 10^{-12}\ \mathrm{m}^2$ and $K_{23.8\%} = 8.236 \pm 0.5 \times 10^{-12}\ \mathrm{m}^2$. Values of absolute permeability for uncompressed non-wet-proof Toray 090 have been experimentally obtained: $K = 12.4 \times 10^{-12}\ \mathrm{m}^2$ [12], $K = 4.4 \times 10^{-12}\ \mathrm{m}^2$ [14], and $K = 9 \times 10^{-12}\ \mathrm{m}^2$ [11]. It is observed that the absolute permeability obtained in the present work is within the range of what is reported by other authors.

Fig. 12 presents the effect of wet-proofing treatment on absolute permeability of GDL materials. It can be readily seen how the absolute permeability is lower for a wet-proof material due to the deposition of PTFE on the fibers; such a deposition reduces the pore size and available space creating a more tortuous path

Table 3
Uncertainty values for absolute permeability determination.

Uncertainty	Value	Units	Notes
$u(\dot{V})$	0.04	sccm	Manufacturer specs.
$u(\Delta x)$	0.05	mm	Machining tolerance
$u(D)$	0.01	mm	Manufacturer specs.
$u(\Delta P)$	0.6225	Pa	Manufacturer specs.

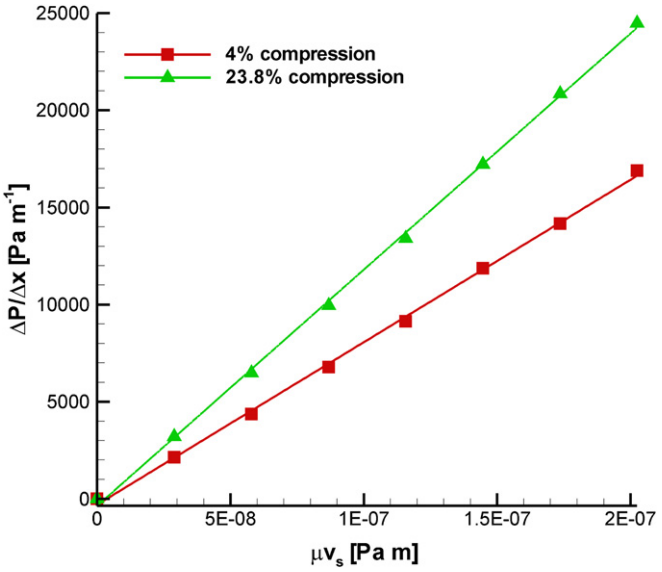

Fig. 11. Effect of compression on absolute permeability in non-wet-proof material.

for a given flow. The absolute permeability obtained for this material (uncompressed) was $K_{20\%\mathrm{PTFE(u)}} = 4.26 \pm 0.11 \times 10^{-12}\ \mathrm{m}^2$, on the other hand, for the compressed version of this material $K_{20\%\mathrm{PTFE(c)}} = 1.098 \pm 0.17 \times 10^{-12}\ \mathrm{m}^2$.

4.4. Relative permeability

The saturation calculation was performed by gravimetric methods for the relative permeability relationships. The saturation was calculated as:

$$S = \frac{\Delta m_{\mathrm{GDL}}}{\frac{\pi}{4}D^2 t\left(\varepsilon_o \frac{t}{t_o}\right)} \tag{14}$$

The difference with respect to the calculation of saturation in the capillary pressure experiments is how the volume imbibed into

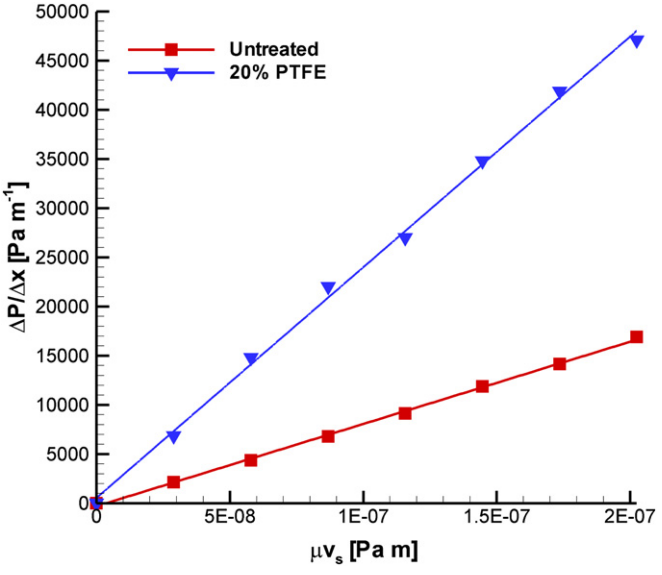

Fig. 12. Effect of wet-proofing on absolute permeability in uncompressed material.

a sample was determined. In the relative permeability experiment, the volume imbibed is calculated as the mass increase of the GDL due to its water content divided by the density of liquid water (ρ_l). In this error analysis the only modification is that there are no uncertainties related to the volume delivered by the pump; however, the mass measurement uncertainty must be added to the values reported in Table 2 as $u(\Delta m_{GDL}) = 0.01$ mg (given by manufacturer).

Liquid phase relative permeability is calculated similarly to absolute permeability; however the experiment required is different because relative permeability is a function of a two-phase flow condition rather than a material property as absolute permeability. Eq. (15) shows the expression used for calculating relative permeability:

$$k_{r,l} = \frac{\mu \dot{V}_l}{KA}\left(\frac{\Delta x}{\Delta P}\right) \tag{15}$$

it can be seen that the same variables and uncertainties determined for absolute permeability apply in the case of relative permeability

Relative permeability is the dimensionless measurement of the effective permeability of a phase in a multi-phase flow through a porous media. Relative permeability is commonly expressed as a function of saturation of the liquid phase; however, it is a more complex function of the fluids properties, matrix properties, history of the system, etc. The functions proposed so far to describe relative permeability of water in GDL material for PEMFCs vary in the literature. The first attempts to evaluate relative permeability were functions proposed that simplified the numerical solution of the water transport problem in fuel cells; later, empirical correlations for well sorted sand were used for PEMFC models; however, just recently, relative permeability has been experimentally determined by Sole [14] and Huassaini and Wang [12].

Regardless of the reference, relative permeability functions for the liquid phase have two similar characteristics. By taking a look at Eq. (15), it can be readily seen that a condition of zero relative permeability is achieved only at zero volumetric flow through a porous material, and because relative permeability is related to a two-phase flow, this limiting condition would represent a single-phase flow of gas where no saturation is present. On the other hand, the maximum value of relative permeability for the liquid phase will be 1 at a condition where the porous media is fully saturated. At this condition, absolute permeability can be determined in a similar fashion as it was described in Section 4.3.

Fig. 13 presents a comparison between relative permeability measurements obtained in this work and those obtained by Huassaini and Wang [12]. Although there are few points in the graph, a little agreement between measurements can be seen at low saturation levels. In Ref. [12], the authors report relative permeability measurements at lower saturation than in the present work; however, in this work, higher saturation levels were attained. More information will be provided in the following paragraphs were the data is presented using error bars.

The effect of wet-proofing on liquid water relative permeability of GDL material is depicted in Fig. 14. It can be observed that the PTFE content in the porous material has a significant impact on the relative permeability function. During the experimentation it was observed that the PTFE-treated material was considerably more difficult to saturate than untreated material. This is confirmed in Fig. 14 where the y-axis can be interpreted as a water flow. Thus, at a given flow condition, it can be observed that is easier to saturate an untreated material than a material treated with PTFE. The experimental data was fitted with functions that held the two conditions described previously and that had a good degree of prediction of the data in between. Surprisingly, Sole [14] obtained

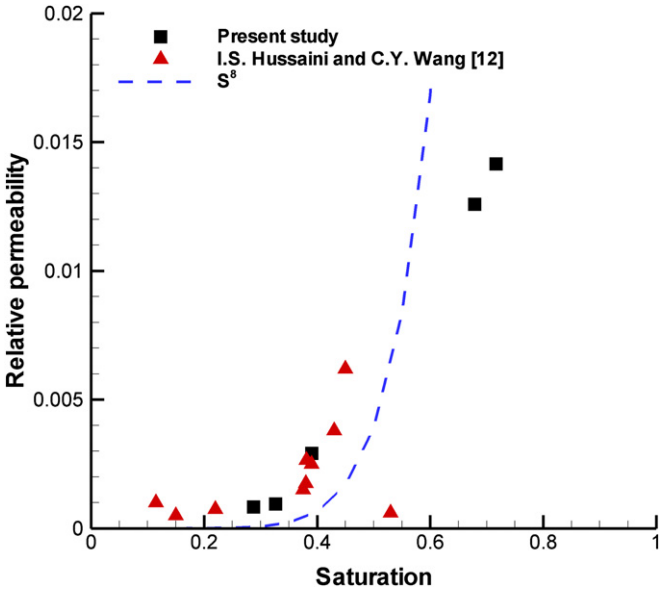

Fig. 13. Comparison of relative permeability measurements, present study versus a previous work.

data with relative low error bars but he used linear functions that did not hold the condition at $S = 1$. Fig. 14 also confirms the observation by Huassaini and Wang [12], that the reliability of the experimental results is hindered due to the large error bars obtained. Huassaini and Wang found that $S^{5.5}$ was a good fit for their experimental results with Toray 090 under a compression of 9%. Conclusions drawn in [12] about liquid water permeability through plane were that further research with more accurate measuring techniques is necessary. In this regards, similar conclusions can be obtained here; however, the functional fittings shown can be used for further numerical models.

Fig. 15 shows the effect of compression (23.8%) on liquid water relative permeability for GDL material with and without wet-proofing. The same tendency observed in the previous figure in regards to the large error bars is repeated in the compression effect study. However, trends can be observed. When a material is

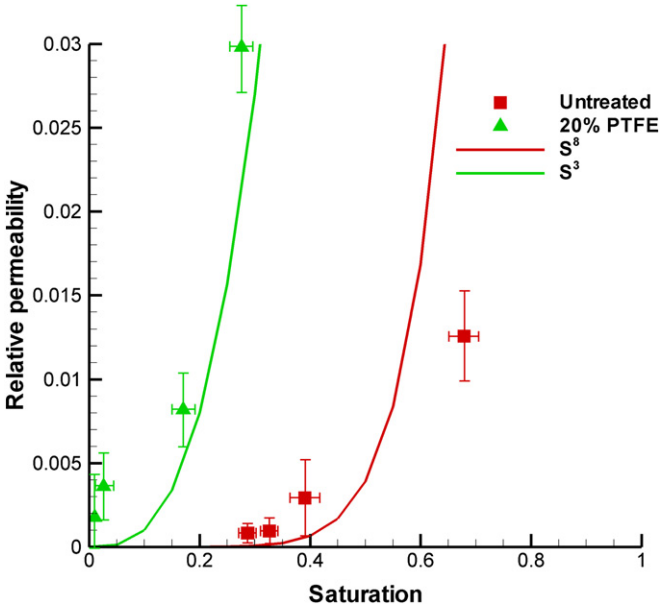

Fig. 14. Effect of PTFE content on liquid phase relative permeability.

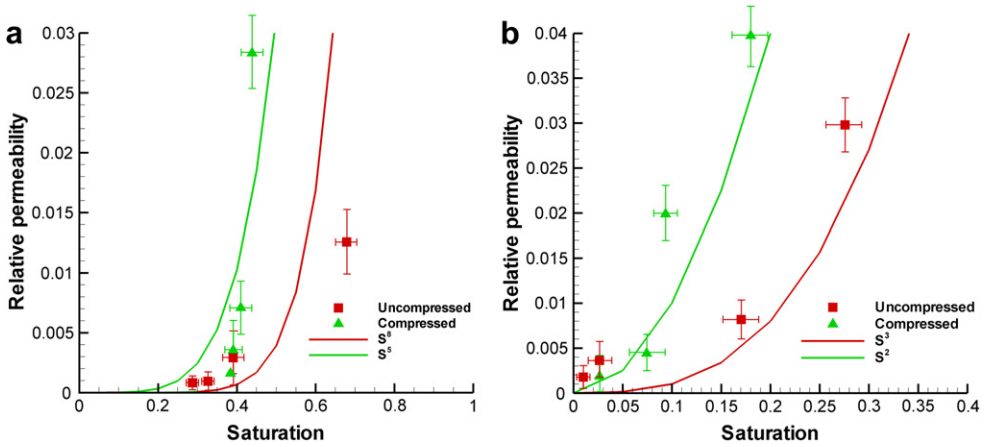

Fig. 15. Study of relative permeability permeability; (a) effect of compression on non-wet-proof material, (b) effect of wet-proofing on uncompressed material.

compressed, the pore space available to hold water is reduced, the thickness is reduced too, and another consequence is the creation of a more tortuous path for the flow. It can be observed that it is more difficult to saturate a material compressed than an uncompressed material at a given flow even when the total thickness is reduced.

5. Conclusions

Much of the continuum modeling approaches reported in the literature use empirical correlations (e.g. Leverett function) for materials like well sorted sand as inputs to the water transport equation. Only recently have researchers begun to develop approaches for the characterization of GDL material in order to provide actual water transport properties such as capillary pressure, porosity, and permeability. In the present work such properties were measured experimentally for Toray 090 carbon paper.

Porosity was determined using the gravimetric and the buoyancy methods. Porosity was measured in materials with different quantities of wet-proofing (PTFE) in their structure. First of all, porosity was obtained for untreated material using the two methods; it was found that the prediction of porosity was very similar to that reported by the manufacturer. Afterwards, porosity was determined for wet-proof materials with 10% and 20% PTFE content. It was observed that porosity decreases as the PTFE content increases. The wet-proofing process consists of sintering PTFE in the porous structure of the diffusion media; hence, the deposition of PTFE reduces the pore space available and the first consequence is the reduction of porosity.

A gas displacement porosimeter designed at Virginia Tech was used to obtain capillary pressure curves of GDL material. The effects of wet-proofing and compression were studied for Toray 090. It was observed that the wet-proofing has a significant effect on capillary pressure curves. It was also found that in order to saturate a wet-proof material, a larger capillary pressure than that for untreated material is required to achieve similar levels of saturation. The resulting effects of wet-proofing on the material were attributed to the modification of the original structure of the GDL due to the deposition of PTFE. The PTFE most likely causes a reduction of the pore space available and, therefore, a reduction of porosity was observed. The wet-proofing also gives hydrophobic properties to the GDL fibers and such a characteristic was observed in the modification of the capillary pressure curves. Similar trends were observed for the compression effect. A compressed material has a lower pore space available and moreover, has smaller pores that require higher pressures to saturate. The creation of a more tortuous path is also a consequence of compression of the GDL. It was experimentally confirmed that compressed materials were more difficult to saturate than uncompressed ones.

Absolute permeability was calculated using a Darcean model and an experimental apparatus designed at Virginia Tech. Absolute permeability is a property of the GDL material and the alteration of this property due to wet-proofing and compression were studied. To measure absolute permeability is a straightforward experiment. A single-phase flow of gas was used as the working fluid. It was observed that absolute permeability decreases due to the reduction of porosity and the creation of a more tortuous path in wet-proof material. Compression exhibited a similar effect. On the other hand, relative permeability turned out to be a difficult property to measure. This is mainly attributed to the assumption on which the experimental apparatus was designed, i.e., the pressure drop for both phases, liquid and gas, is the same. Also, the creation of a two-phase flow system was found to be difficult. However, some trends were observed in terms of wet-proofing and compression. It was found that wet-proofing reduces the amount of saturation achieved at a given flow condition and compression also showed the same result. Fittings were performed for this property as a function of saturation; however, low accuracy was obtained due to the high experimental error observed.

The addition of a backing layer or micro-porous layer (MPL), to the gas diffusion layer of PEMFCs has been reported as an effective way to address the water management problem. Therefore, in the future, experimental characterization of the MPL would be useful for the development of more comprehensive models of PEM fuel cells. The present work presents guidelines and equipment to conduct such analysis and this is left as an opening for further works.

The results presented here provide the PEMFC research community with a greater understanding of GDL transport properties and more complete data for the correct modeling of water transport in fuel cells, thus reducing the need for to rely on assumptions and empirical correlations from other fields.

Acknowledgments

This work was conducted at the Institute for Critical Technology and Applied Science at Virginia Polytechnic Institute and State University under the guidance of Prof. Michael W. Ellis. The first author was able to work on this project thanks to the sponsorship provided by the Mexican National Council on Science and Technology (CONACYT) and the University of Guanajuato.

References

[1] Chun-Hua Min, A novel three-dimensional, two-phase and non-isothermal numerical model for proton exchange membrane fuel cell, J Power Sources 195 (2010) 1880–1887.

[2] C.Y. Wang, P. Cheng, A multiphase mixture model for multiphase, multi-component transport in capillary porous media I: model development, Int J Heat Mass Tran 39 (1996) 3607–3618.

[3] Wensheng He, Jung S. Yi, Trung Van Nguyen, Two-phase flow model of the cathode of PEM fuel cells using interdigitated flow fields, AIChE Journal 46 (2000) 2053–2064.

[4] Dilip Natarajan, Trung Van Nguyen, A two-dimensional, two-phase, multi-component, transient model for the cathode of a proton exchange membrane fuel cell using conventional gas distributors, J Electrochem Soc 148 (2001) 1324–1335.

[5] Jeffrey T. Gostick, Michael W. Fowler, Marios A. Ioannidis, Mark D. Pritzker, Y.M. Volfkovich, A. Sakars, Capillary pressure and hydrophilic porosity in gas diffusion layers for polymer electrolyte fuel cells, J Power Sources 156 (2006) 375–387.

[6] Joseph D. Fairweather, Perry Cheung, Jean St-Pierre, Daniel T. Schwartz, A microfluidic approach for measuring capillary pressure in PEMFC gas diffusion layers, Electrochem Commun 9 (2007) 2340–2345.

[7] T. Jeff Gostick, A. Marios Ioannidis, W. Michael Fowler, D. Mark Pritzker, Direct measurement of the capillary pressure characteristics of water–air–gas diffusion layer systems for PEM fuel cells, Electrochem Commun 10 (2008) 1520–1523.

[8] T. Jeff Gostick, A. Marios Ioannidis, W. Michael Fowler, D. Mark Pritzker, Wettability and capillary behavior of fibrous gas diffusion media for polymer electrolyte membrane fuel cells, J Power Sources 194 (2009) 433–444.

[9] T. Jeff Gostick, A. Marios Ioannidis, W. Michael Fowler, D. Mark Pritzker, On the role of the microporous layer in PEMFC operation, Electrochem Commun 11 (2009) 576–579.

[10] I.R. Harkness, N. Hussain, L. Smith, J.D.B. Sharman, The use of a novel water porosimeter to predict the water handling behaviour of gas diffusion media used in polymer electrolyte fuel cells, J Power Sources 193 (2009) 122–129.

[11] T. Jeff Gostick, W. Michael Fowler, D. Mark Pritzker, A. Marios Ioannidis, M. Leya Behra, In-plane and through-plane gas permeability of carbon fiber electrode backing layers, J Power Sources 162 (2006) 228–238.

[12] I.S. Hussaini, C.Y. Wang, Measurement of relative permeability of fuel cell diffusion media, J Power Sources 195 (2010) 3830–3840.

[13] Jörg Roth. Water transport in gas diffusion media for PEM fuel cells: experimental and numerical investigation, doctoral dissertation, Universität Duisburg-Essen, 2010.

[14] J.D. Sole. Investigation of water transport parameters and processes in the gas diffusion layer of PEM fuel cells, Doctoral dissertation, Virginia Polytechnic Institute and State University, 2008.

[15] Hyunchul Ju, Analyzing the effects of immobile liquid saturation and spatial wettability variation on liquid water transport in diffusion media of polymer electrolyte fuel cells (PEFCs), J Power Sources 185 (2008) 55–62.

[16] T. Jeffrey Gostick, A. Marios Ioannidis, W. Michael Fowler, D. Mark Pritzker, Characterization of the capillary properties of gas diffusion media, Modern Aspects of Electrochemistry 49 (2010) 225–254.